Digital Object Identifier 10.1109/TPEL.2022.3191428

IEEE Transactions on Power Electronics

State-Feedback Reshaping Control of Voltage Source Converter

Federico Cecati

Rongwo Zhu

Sante Pugliese

Marco Liserre

Xiongfei Wang

Suggested Citation

F. Cecati, R. Zhu, S. Pugliese, M. Liserre and X. Wang, "State-Feedback Reshaping Control of Voltage Source Converter," in IEEE Transactions on Power Electronics, 2022, doi: 10.1109/TPEL.2022.3191428.

State-Feedback Reshaping Control of Voltage Source Converter

Federico Cecati, *Student Member, IEEE*, Rongwu Zhu, *Member, IEEE*, Sante Pugliese, *Member, IEEE*, Marco Liserre, *Fellow, IEEE*, Xiongfei Wang *Senior Member, IEEE*

***Abstract*—Admittance reshaping is a widely used strategy to address the converters low-frequency stability issues in weak grid, caused by the PLL and its interaction with the dc and ac voltage control. However, the asymmetric control of the d- and q-axis current references and the coupling between the converter ac and dc side restricts the damping capability of Single-Input-Single-Output feedbacks. This phenomena gets even worse in presence of nearby converters. This paper extends the concept of admittance reshaping to Multi-Input-Multi-Output (MIMO) control. A full state-feedback is added to the current reference of the converter to increase the damping of the conventional multi-loop control. A systematic offline algorithm is delegated to design the feedback, and a scalar coefficient is employed to activate/deactivate online the reshaping feedback, making the proposed solution user-friendly. The proposed control is analyzed both in time- and frequency-domain and tested in parallel-operation with other converters, and shows higher damping capability than conventional solutions and good robustness with respect to grid impedance and operating point variations. Experimental tests under ac and dc disturbances are conducted both in lab setup and in Hardware-In-the-Loop.**

***Index Terms*—State-Feedback, Reshaping Control, Low Frequency Stability, Voltage Source Converter, Active Damping**

I. Introduction

THE evolution of the distribution and transmission grid towards a power electronics-dominated network brings new challenges for the stability [1], [2]. Low-frequency stability problems in grid-following voltage source converters (VSCs) are mainly related to the outer control loops, e.g. the synchronous reference frame phase-locked loop (SRF-PLL) [3], the dc voltage control (DVC) [4], the ac voltage control (AVC) [5]. Recent studies highlighted that the *interaction* between PLL, DVC and AVC, besides their individual dynamics, is a major cause of instability [6]–[8]. This represents a challenge for the control design [9]–[13].

Damping is a fundamental concept in VSC stability and control [14], [15]. Low damped converter dynamics result in poor stability margins, high overshoot, large and persistent oscillations, which jeopardize the stability of the rest of the grid [1], [15], [16]. In dynamic systems, e.g. VSCs, the damping ratio around an equilibrium point can be determined by the eigenvalues of the Jacobian A matrix, and highly depends on the control tuning parameters [7], [8]. Decreasing the PLL bandwidth has been demonstrated to increase the VSC damping in weak grid, yet it impairs the VSC response to fast grid transients [8], [17], [18]. Substituting the PLL with a power synchronization also improves the damping in weak grids, yet it may introduce stability problems in stiff grid [19], [20]. Another widely used approach is to add an active damping (AD) feedback u in the current reference of the converter *main* control, as shown in Fig. 1 in generic form [9], [21].

The AD feedback u is often designed in the frequency domain with the aim of "reshaping" the converter output admittance to enhance the stability. This strategy is often called admittance (or impedance) reshaping [14], [22]–[24]. In many cases, the feedback variable ξ in Fig. 1 is a voltage, and the transfer function $K(s)$ assumes the meaning of a virtual admittance [9], [14], [21].

Virtual admittance design and stability analysis are often realized through Single-Input-Single-Output (SISO) approaches, neglecting the d-q axes cross-coupling [9], [14], [22], [23]. The paper [11] pointed out that the d-q axes cross-coupling due to the SRF-PLL cannot be neglected, and proposed a symmetrical PLL to eliminate the coupling and allow SISO impedance reshaping design. Nevertheless, it neglects the DVC and AVC, which also creates d-q axes cross-coupling [25], [26]. The drawback of neglecting the dynamics coupling to simplify the virtual admittance design is that the resulting AD control increases the damping in limited amount [25], [26]. In grids with high penetration of power converters and low SCR, high amount of damping are requested for a stable and smooth response to disturbances [17]. Conventional SISO solutions in these cases may be insufficient, leading to persistent oscillations in the grid and low stability margins [7]. That motivated to redesign the entire VSC control system through Multi-Input-Multi-Output (MIMO) techniques [25], [26].

Besides these aspects related to the ac side stability, the VSC stability can be threatened also by disturbances coming from the dc side [27], often neglected in literature [9], [14], [21]. In order to include dc terminals in the model and analyze its interaction with the ac side, the VSC has to become a 3×3 MIMO system, making the stability analysis and control even more difficult. Lastly, the VSC dynamics nonlinearity is a further challenge, since the equivalent damping of the VSC can change depending on the operating point [7], [27]. Therefore, a method for computing the VSC equilibrium point (and assess if it *exists*) must be determined, and a nonlinear model which can be linearized around different operating conditions (grid voltage level, VSC active power level, grid impedance) has to

be employed.

This paper extends the idea of admittance reshaping to MIMO control. A nonlinear MIMO VSC model with 3 inputs (dc current and dq grid voltage) and 3 outputs (dc voltage and dq ac current) is derived. An AD state-feedback u is designed and applied to the current loop reference as in Fig. 1, considering as ξ the n-dimensional VSC state vector, and as $K(s)$ a low-pass filtered $2 \times n$ gain matrix K. The control is designed based on eigenvalue placement [28] applied to the plant highlighted in the red frame in Fig. 1, composed of the VSC, its main control and the grid Thevenin equivalent. The full state-feedback allows to *arbitrarily* set the damping ratio and natural frequency of all the closed loop eigenvalues, and will be demonstrated to have higher AD capability than conventional SISO admittance reshaping.

An *offline* systematic and user-friendly algorithm is entirely delegated to design the state-feedback matrix K, and a reshaping coefficient σ is added to the control law to easily activate/deactivate the reshaping feedback. The effect of the reshaping control on the dc side dynamics and the interactions with the ac side is studied through frequency domain analysis, showing an effective AD action for the resonances. The nonlinear VSC model is linearized around different equilibrium points, computed through Newton-Raphson method, to analyze the damping capability during different grid SCR (from 4.5 down to 1.1), grid voltage and VSC active power levels. The proposed reshaping control is analyzed and tested also in parallel operation with other VSCs, showing in each case higher damping capability than conventional solutions [9]. Experiments are conducted both in a lab setup and in Hardware-In-the-Loop, and demonstrate that the proposed control increases the damping in multi-VSC microgrids and stabilize them during various kinds of disturbances, both coming from the ac and dc converter side.

The paper is structured as follows: section II describes the VSC modeling and linearization, section III the control design, section IV presents the frequency-domain analysis, section V analyses the robustness, section VI shows the experimental results, and section VII presents the conclusions.

II. Fundamentals of Reshaping Control and Model Derivation

The scheme of the considered L-filtered three-phase VSC is depicted in Fig. 1. The converter is supplied by an upstream primary energy source modeled with a current source injecting a current $i_{dc} = \frac{P^*}{v_{dc}}$, where P^* is the generated active power. The converter *main* control, highlighted in the yellow frame in Fig. 1, is the conventional multi-loop control [2], [8], including a PI controller for the dc-link voltage, a PI controller for the ac voltage magnitude and a synchronous reference frames phase-locked-loop (SRF-PLL) for the synchronization; the reference current is tracked through a PI inner current loop. The VSC is connected to the grid, modeled with a voltage source e with a series impedance Z_g.

The key feature of the state-feedback *reshaping* control is the plant used for the control design, highlighted in the red frame in Fig. 1. The inclusion of the complete *main* control model (i.e. PLL, voltage and current controllers) in the plant is essential to reshape its dynamics, and distinguishes the proposed reshaping control from other MIMO controls in literature [25], [26]. The resulting AD state-feedback will thus contain also states from the VSC main control, as explained in the next section. The inclusion of the grid Thevenin equivalent model with a high impedance Z_g in the plant is instead needed to capture the mechanism of grid-following instability in weak grid condition, and to design proper reshaping feedback to mitigate it. The equivalent grid impedance is modeled as a RL branch $Z_g(s) = R_g + sL_g$, as by most of the researches focusing on low frequency dynamics [9], [11], [29]. Nevertheless, Z_g is often uncertain and time-variant, and is furthermore influenced by the presence of other converters in the nearby, representing a great challenge for the control design [30]. Therefore, it is necessary to investigate if the proposed state-feedback reshaping control designed under a certain value of $Z_g(s)$ is robust, i.e. it can keep its damping properties also under a different Z_g and in presence of other parallel connected converters.

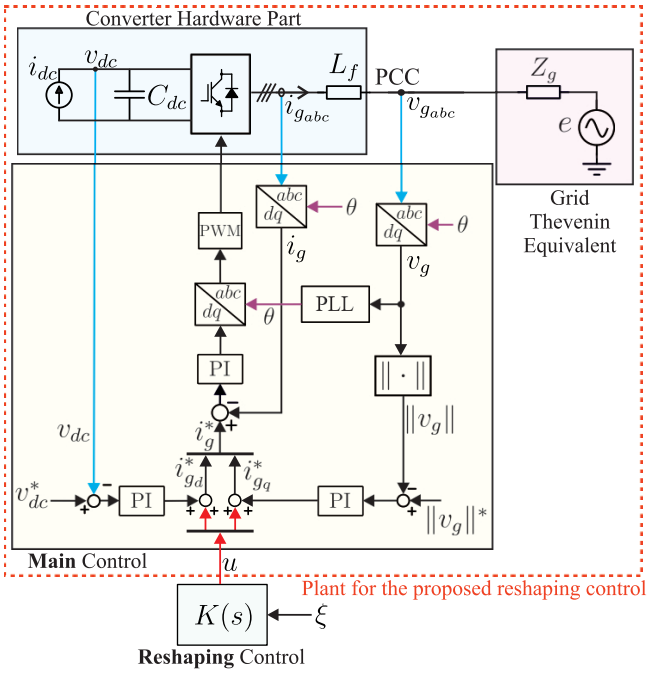

Fig. 1: The three-phase voltage source converter with the addition of a generic reshaping control feedback.

A. Converter nonlinear modeling

The proposed reshaping control aims to damp the dynamics in the near- and sub-synchronous frequency range. Thus, the model used for the control design needs to include only the dynamics responsible of the oscillations in this frequency range, i.e. the outer loops and the ac/dc power conversion [1], [8]. We proposed and validated in [7], [31] a novel current loop dq-frame model for low frequency dynamic analysis of power systems, which is particularly suitable for the design of the low-frequency state-feedback reshaping control. The main

idea of [7], [31] is to model inverter ac side and its current loop with a Norton equivalent, whose state-space model is:

$$\begin{cases} \dot{v}_{cc} = K_i i_c - K_i i_g \\ \dot{i}_c = -\omega_{cc} i_c + \omega_{cc} i_g^* \\ v_g = K_p \left(i_c - i_g \right) + v_{cc} \end{cases} \tag{1}$$

The derivation of (1) follows the typical mathematical steps used in impedance-based modeling [8], yet it expresses the final result in state-space form. Further details can be found in [7], [31].

The model (1) of the current loop can be merged together with the model of the dc-link dynamics and the outer loops, obtaining the VSC state-space model:

$$\begin{cases} \dot{x} = f(x, u, d, r) \\ y = h(x, u, d, r) \end{cases} \tag{2}$$

where the state vector x, the reshaping control input u, the disturbance input d, the reference input r, and the output y are defined respectively as:

$$\begin{cases} x = \begin{pmatrix} i_c & v_{dc} & \Phi_{dc} & \Phi_g & \delta & \Phi_q & v_{cc} & i_g \end{pmatrix}^T \\ u = \begin{pmatrix} u_d & u_q \end{pmatrix}^T \\ d = \begin{pmatrix} i_{dc} & e \end{pmatrix}^T \\ r = \begin{pmatrix} v_{dc}^* & v_g^* \end{pmatrix}^T \\ y = \begin{pmatrix} v_{dc} & i_g \end{pmatrix}^T \end{cases} \tag{3}$$

The *reshaping* control input u has the dimension of a current in dq frame, and is added to the current control reference i_g^* as in Fig. 1. The model (2) expressed by nonlinear differential equations is:

$$\begin{pmatrix} \dot{i}_c \\ \dot{v}_{dc} \\ \dot{\Phi}_{dc} \\ \dot{\Phi}_g \\ \dot{\delta} \\ \dot{\Phi}_q \\ \dot{v}_{cc} \\ \dot{i}_g \end{pmatrix} = \begin{pmatrix} -\omega_{cc} i_c + \omega_{cc} i_g^* \\ -\frac{3}{2} \frac{1}{C_{dc}} \frac{v_g \cdot i_g}{v_{dc}} + \frac{1}{C_{dc}} \frac{P^*}{v_{dc}} \\ v_{dc} - v_{dc}^* \\ v_g^* - \sqrt{v_g \cdot v_g} \\ \begin{pmatrix} 0 & K_{p,PLL} \end{pmatrix} v_g + K_{i,PLL} \Phi_q \\ \begin{pmatrix} 0 & 1 \end{pmatrix} v_g \\ -K_i i_g + K_i i_c \\ -\frac{R_g}{L_g} i_g - \Omega i_g + \frac{1}{L_g} v_g - \frac{1}{L_g} T(\delta) e \end{pmatrix} \tag{4}$$

with

$$\begin{cases} v_g = K_p \left(i_c - i_g \right) + v_{cc} \\ i_g^* = \begin{pmatrix} K_{p,DC} \left(v_{dc} - v_{dc}^* \right) + K_{i,DC} \Phi_{dc} \\ K_{p,AC} \left(v_g^* - \sqrt{v_g \cdot v_g} \right) + K_{i,AC} \Phi_g \end{pmatrix} + u \\ T(\delta) = \begin{pmatrix} \cos\delta & \sin\delta \\ -\sin\delta & \cos\delta \end{pmatrix} \\ \Omega = \begin{pmatrix} 0 & -\omega \\ \omega & 0 \end{pmatrix} \end{cases} \tag{5}$$

The obtained model (4)-(5) is linearized and used to design the proposed state-feedback reshaping control.

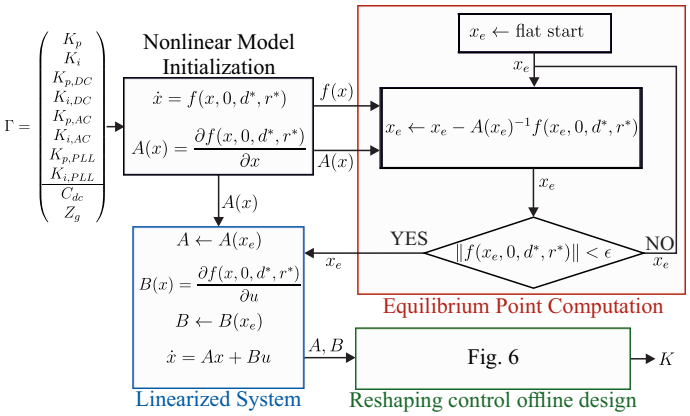

Fig. 2: The offline procedure for the computation of the VSC equilibrium point and linearization.

B. Equilibrium point computation and model linearization

For the linearization of the model (2), two important concepts must be distinguished: *operating* point and *equilibrium* point [7]. The *operating* point of the VSC is determined by the steady-state values of the converter inputs d and r in (3), denominated d^* and r^* respectively. The operating point defines the conditions on which the converter is operating, particularly its nominal active power, the grid voltage e level and the set-points of the control system. The *equilibrium* point is the steady-state value of the VSC state x in (3), denominated x_e, when the converter is working at the operating point defined by d^* and r^* [17].

It is important to remark that the equilibrium point does not always exist [32]. By increasing the active power P^*, i.e. increasing i_{dc} in d^*, if the static power transfer limit is exceeded the equilibrium point does not exist and the system gets unstable [33]. Also in low grid voltage e scenarios, e.g. sustained voltage sags, the non-existence of the equilibrium point has been widely reported as a cause of instability [17], [34]. This kind of instability is different from small-signal instability and is out of the object of this paper: the operating points where the equilibrium point does not exist will be excluded from all the following analyses.

The authors proposed in [7] the use of Newton-Raphson algorithm on the nonlinear model (2) to compute (if existing) the VSC equilibrium point and obtain a linearized model. The procedure, which has to be run *offline* before the control design, is explained in Fig. 2. The converter nonlinear model (4)-(5) is initialized with its main hardware and control parameters given as input in form of an array Γ, and its operating point given by d^* and r^* is substituted into the model. The reshaping input u is set to 0, since it does not affect the equilibrium point [12]. The Jacobian matrix $A(x)$ is then computed with the help of symbolic computational toolbox [35]. A flat start for x_e is chosen by considering $v_{dc} = v_{dc}^*$, $v_{cc} = v_g^*$ and the other state variables null, the Newton-Raphson algorithm is executed, and the equilibrium point x_e is computed [7]. In the case when the equilibrium point does not exist due to exceeded static power transfer limit, the Newton-Raphson algorithm did not converge, as expected [32].

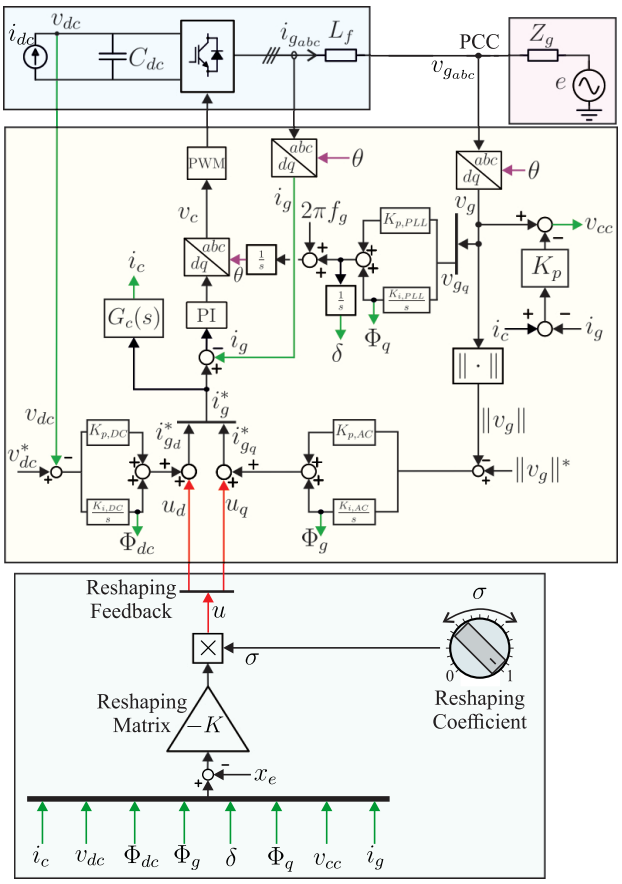

Fig. 3: The implementation of the proposed state-feedback reshaping control in the VSC.

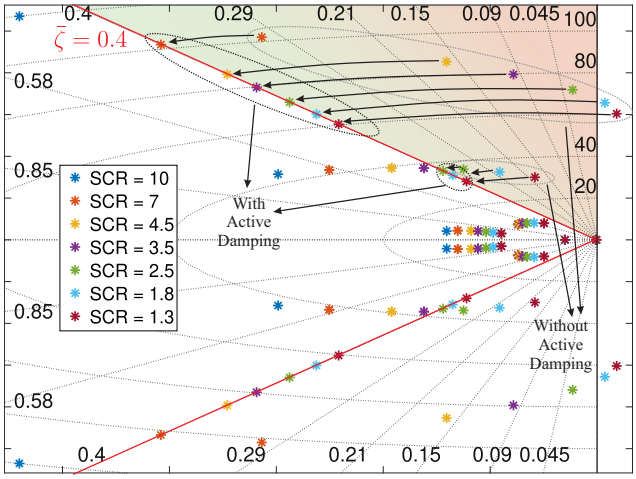

Fig. 4: The effect of the reshaping feedback on the closed loop eigenvalues at different SCR values.

III. State-Feedback Reshaping Control

The AD feedback u is applied to the current loop reference i_g^* similarly to a virtual impedance, as shown in red in Fig. 3. The proposed reshaping control has the form of a modified full state-feedback:

$$u = -\sigma K \left(x - x_e \right) \tag{6}$$

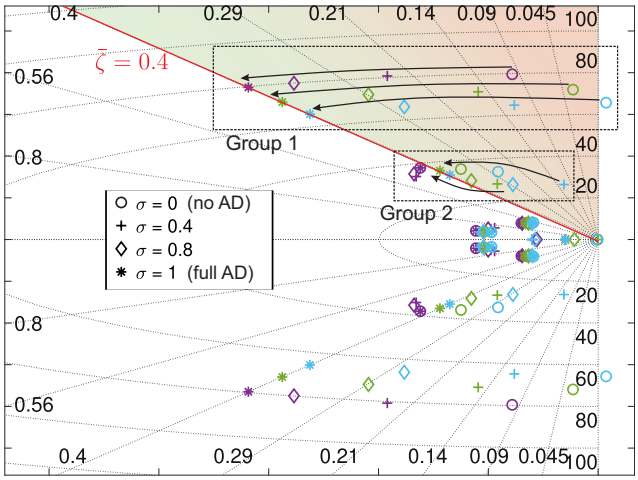

Fig. 5: The effect of the reshaping coefficient σ on the closed loop eigenvalues for SCR = 3.5, SCR = 2.5, SCR = 1.8.

Three main constituent elements are present in the reshaping control law (6), discussed in detail in section III-A:

1) K is the 2×11 feedback gain matrix (denominated *reshaping matrix*)
2) σ is a scalar coefficient (denominated *reshaping coefficient*) between 0 and 1
3) x_e is a feed-forward term, and can be chosen either as the flat start discussed in subsection II-B, or as the equilibrium point computed through the procedure in Fig. 2.

Considering $\sigma = 1$, the control law (6) is a conventional state-feedback law, which arbitrarily assigns the eigenvalues position of the closed loop state matrix $(A - BK)$ [16], placed in this case in a well-damped position ($\zeta = \bar{\zeta}$) as shown in Fig. 4. By adjusting σ in the interval $[0, 1]$ in (6), the closed-loop eigenvalues position can be further regulated, as shown in Fig. 5. For $\sigma = 0$, the reshaping feedback is completely deactivated, resulting in the traditional multi-loop control [8]. By increasing σ the eigenvalues follows a trajectory toward the desired position established through K, reached for $\sigma = 1$. This strategy has a precise reason: acting directly on the matrix K to change VSC behaviour is not intuitive, it requires a deep control theory experience and cannot be done online. Instead, using a scalar coefficient σ to switch on/off and regulate the damping action fixed by the term $-K\left(x - x_e\right)$ in (6), *also online*, provides a unique effectiveness/usability profile. From the effectiveness point of view, the full state-feedback (6) has total dynamics reshaping capability [16]. From the usability point of view, the amount of damping is regulated through a single parameter $\sigma \in [0, 1]$. To make the proposed control even more user-friendly, the design of the matrix K can be made *systematic*, i.e. a set of design guidelines and rules applicable by an offline algorithm which requires a minimal human intervention can be defined.

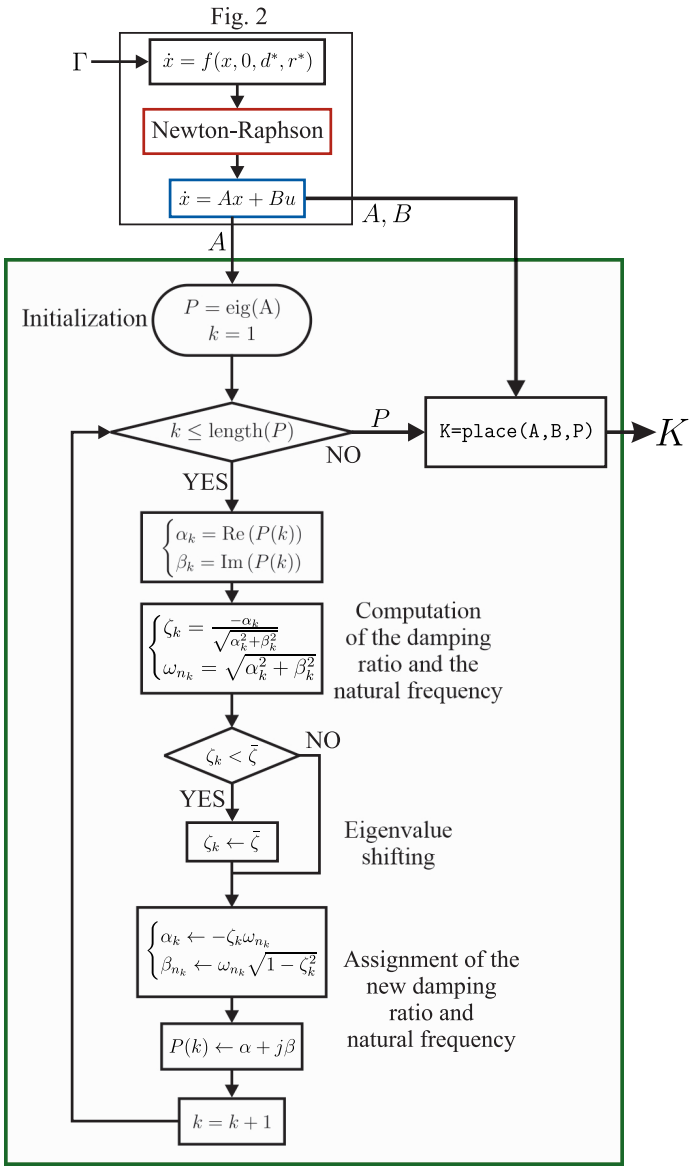

Fig. 6: The flowchart of the proposed offline algorithm for the reshaping control law design.

A. Systematic Offline Algorithm for Reshaping Control Design

The proposed systematic design algorithm for the reshaping matrix K is shown in Fig. 6. The linearized VSC model is derived through the procedure explained in section II, and embedded in the algorithm. The VSC main hardware and control parameters are set in the model through the array Γ. The resulting reshaping control law (6) is thus tailored to the parameters declared in Γ. The grid impedance Z_g inside Γ can be however uncertain and time-variant [30], yet a robust initialization rule will be proposed in section V, so that the reshaping control must not be redesigned if Z_g varies. The tuning of the main control has to be realized according to the well-known guidelines proposed in literature [2], [8]. It is not necessary to tune the outer loops, e.g. the PLL, with lower bandwidth in order to have higher damping in weak grid condition, since a significant amount of damping is already introduced by the reshaping control.

The systematic rule for the choice of the closed-loop eigenvalues position P relies on a control theory result presented in the book [15]: the time-domain equivalent of a phase margin of $45°$ is a minimum eigenvalue damping of $\zeta = 0.4$, which ensures a sufficient stability margin [8]. From that, the rule implemented by the algorithm in Fig. 6 can be defined:

Design Rule. *The closed-loop eigenvalues are chosen to have a damping ratio equal or higher than $\bar{\zeta} = 0.4$ for all of them, using the minimum possible control effort to achieve it. Thus:*

- *The eigenvalues with a damping ratio ζ lower than $\bar{\zeta}$ are moved to the locus $\zeta = \bar{\zeta}$ without modifying their natural frequency.*
- *The eigenvalues which already have a damping higher than $\bar{\zeta}$ are not moved, in order to not fruitlessly increase the control effort.*

The eigenvalue placement is graphically explained in Fig. 4. The critical damping $\bar{\zeta} = 0.4$ is represented with the red line. With SCR$= 10$, all the eigenvalues are already well-damped, thus no active damping is required, and the matrix K is computed as null by the algorithm. With SCR ≤ 7, some eigenvalues go beyond the red line, i.e. have a damping ratio lower than $\bar{\zeta} = 0.4$; in this case, the AD state-feedback shifts them back to the red line ($\zeta = \bar{\zeta}$), without changing their natural frequency.

From the obtained eigenvalues position P, the reshaping matrix K is computed though a standard eigenvalue placement routine [28] implemented through the function `K=place(A,B,P)` in Matlab®, applied to the nonlinear model (2) linearized around the nominal operating point ($e = 1$ p.u., $P^* = 1$ p.u.). The variation of the operating point does *not* require the re-computation of the matrix K, as it will be demonstrated in the next section.

Fig. 5 analyzes the VSC dynamics with the reshaping coefficient σ between 0 and 1, and demonstrates that σ acts as a *knob* to flexibly regulate the AD intensity, as graphically represented in Fig. 3. In most of the cases, the converter is desired to operate either with $\sigma = 1$ (full AD) or $\sigma = 0$ (no AD), nevertheless when adjusting σ *online*, i.e. with the VSC under operation, it is recommended to vary it *progressively* in order to avoid abrupt transients.

B. Control Implementation

The reshaping control law (6) needs the state variables of x as defined in (3), highlighted in Fig. 3 with green arrows. Some states, e.g. v_{dc} and i_g, are directly available from the measurement sensors. Other states, e.g. Φ_{dc}, Φ_g, Φ_q, are the integral states of the PI dc-link voltage control, the ac voltage control and the PLL respectively, and can be taken from the VSC main multi-loop control, without additional computations. Other state variables, e.g. i_c, δ and v_{cc} needs to be generated through simple operations on the existing variables, according to (4)-(5). The variable i_c is obtained in Fig. 3 as $i_c = G_c(s) i_g^*$ with $G_c(s) = \frac{\omega_{cc}}{s+\omega_{cc}}$, which is the Laplace transform of the differential equation

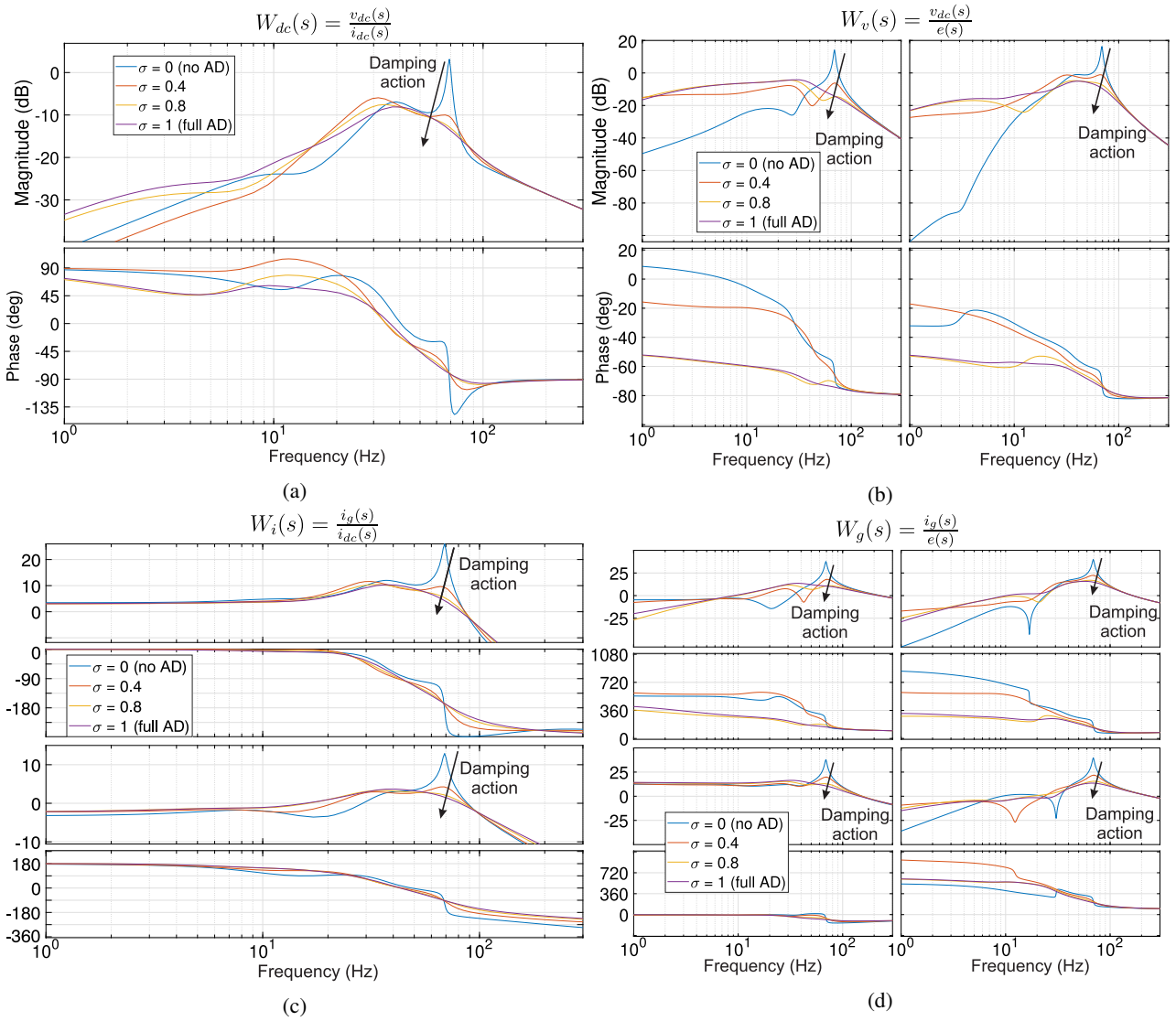

Fig. 7: The frequency response of the grid-connected converter with reshaping control. (a) $W_{dc}(s)$. (b) $W_v(s)$. (c) $W_i(s)$. (d) $W_g(s)$.

$\dot{i}_c = -\omega_{cc} i_c + \omega_{cc} i_g^*$ defined in (4). δ is obtained by integrating the output of the PLL, according to the definition of $\dot{\delta}$ in (4). v_{cc} is obtained as $v_{cc} = v_g - K_p(i_c - i_g)$ from (5).

IV. Frequency-Domain Analysis of Reshaping Control

The transfer function $W(s)$ of the model (2) linearized around its equilibrium point can be computed for frequency domain analysis of the reshaping control, as follows:

$$W(s) = C\left(sI - (A - \sigma BK)\right)^{-1} E + F \tag{7}$$

where A and B have been computed according to Fig. 2, and

$$\begin{cases} C = \left.\dfrac{\partial h(x,0,d^*,r^*)}{\partial x}\right|_{x=x_e} \\ E = \left.\dfrac{\partial f(x,0,d^*,r^*)}{\partial d}\right|_{x=x_e} \\ F = \left.\dfrac{\partial h(x,0,d^*,r^*)}{\partial d}\right|_{x=x_e} \end{cases} \tag{8}$$

$W(s)$ is a 3×3 transfer function which can be written as

$$\begin{pmatrix} v_{dc}(s) \\ i_{g_d}(s) \\ i_{g_q}(s) \end{pmatrix} = \left(\begin{array}{c|cc} W_{11}(s) & W_{12}(s) & W_{13}(s) \\ \hline W_{21}(s) & W_{22}(s) & W_{23}(s) \\ W_{31}(s) & W_{32}(s) & W_{33}(s) \end{array}\right) \begin{pmatrix} i_{dc}(s) \\ e_d(s) \\ e_q(s) \end{pmatrix} \tag{9}$$

in compact form:

$$\begin{pmatrix} v_{dc}(s) \\ i_g(s) \end{pmatrix} = \begin{pmatrix} W_{dc}(s) & W_v(s) \\ W_i(s) & W_g(s) \end{pmatrix} \begin{pmatrix} i_{dc}(s) \\ e(s) \end{pmatrix} \tag{10}$$

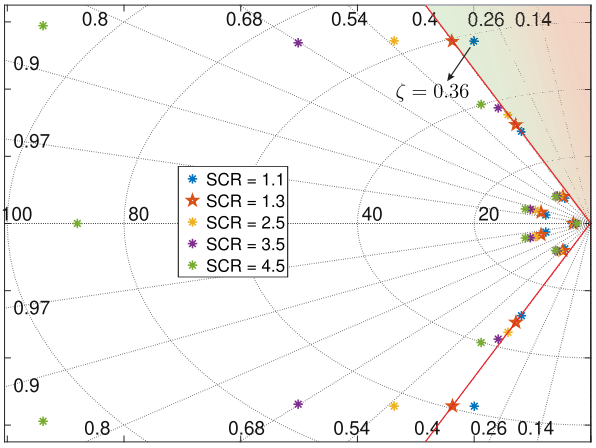

Fig. 8: The eigenvalues of the VSC with reshaping control designed for SCR= 1.3 (highlighted with the star) under different SCR values.

In (10), both dc quantities (i.e. i_{dc}, v_{dc}) and ac quantities expressed in dq frame (i.e. e, i_g) are involved, and their cross-coupling is described by the off-diagonal matrices $W_i(s)$ and $W_v(s)$. The following analysis is *not* meant to be a impedance-based stability analysis as in other papers in literature [21], [23], [24], rather a tool to evaluate the converter frequency response to disturbances coming from the dc side of the VSC and the ac grid. The stability in this paper is *always* assessed through time-domain eigenvalue analyses, as in Figs. 4,5.

Fig. 7 shows the bode plot of the four block matrices of $W(s)$ expressed in (10) under a SCR=2.5, where according to Fig. 4 the VSC is small-signal stable but with low damped dynamics. Low damped eigenvalues result in sharp resonances in the frequency domain in all the nine transfer functions of $W(s)$, as shown in Fig. 7, which bring large and persistent oscillations, high overshoot and poor stability margin, both during ac grid disturbances and dc side disturbances [15]. The reshaping control can damp all the resonances and ensure a smooth converter frequency response, with low overshoot, well-damped oscillations and high stability margin, as shown in Fig. 7. In $W_v(s)$ in Fig. 7(b), a higher magnitude in the low frequency range when using the reshaping control can be noticed. This effect slightly impacts the settling time of the dc voltage control when subject to disturbance from the ac grid, but does not represent a practical issue for the dc voltage tracking and stability.

It is important to remark that, $W_g(s)$ in Fig. 7(d) must not be confused with the converter output admittance used by many papers for impedance-based stability analyses, since it is computed with respect to the grid voltage e and depends also on the grid impedance Z_g [9], [22], [36].

V. Performance Analysis of State-Feedback Reshaping Control

This section firstly analyzes the performance of the proposed MIMO reshaping control under SCR and operating point variations. Afterwards, an analysis of the behaviour of the reshaping control in presence of other VSCs connected in the nearby is carried out. The results are compared with conventional SISO solutions proposed in literature [9], [14].

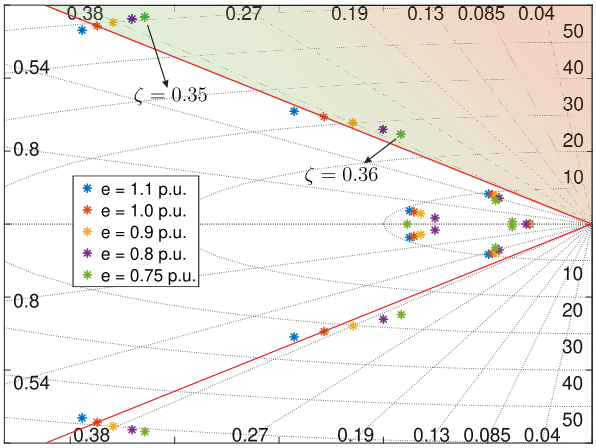

(a)

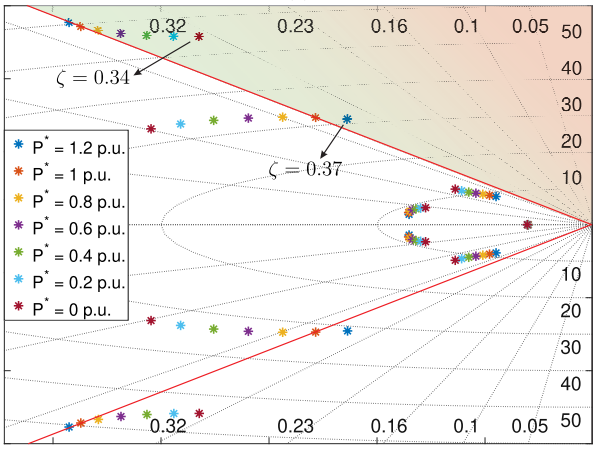

(b)

Fig. 9: The robustness of the reshaping control under operating point variations. (a) Grid voltage e level variation. (b) Active power reference P^* variations.

TABLE I: VSC-based wind turbine and grid parameters

Parameters	Values
Line-to-line grid voltage (V)	690
R/X ratio	0.3
Power rating (MW)	4
DC-link voltage (V)	1200
Switching frequency (kHz)	2
DC-link capacitor (mF)	22
Filter inductor (mH)	0.1

A. Robustness under SCR and operating point variations

The reshaping control design discussed in the previous sections is done by considering a grid Thevenin equivalent, shown in Fig. 1, with an equivalent resistive-inductive impedance Z_g. In real grids, Z_g can vary depending on the grid configuration, and can be affected by other VSCs connected in the nearby [37].

The eigenvalue analysis in Fig. 8 considers a VSC with reshaping control designed for a SCR equal to 1.3 (highlighted with the star), and studies its dynamics both in the case of

TABLE II: Parameters of the VSC-based power system shown in Fig. 10

Main grid parameters			**Values**
Line-to-line grid voltage (V)			690
R/X ratio			0.3
Short Circuit Ratio			1.3
VSCs parameters	**VSC 1**	**VSC 2**	**VSC 3**
Injected Active Power (MW)	1	1.2	0.8
DC-link voltage (V)	1200	1200	1200
Switching frequency (kHz)	2	2	2
DC-link capacitor (mF)	22	20	22
Filter inductor (mH)	0.1	0.1	0.1
PLL settling time (s)	0.2	0.2	0.18
Reshaping virtual admittance Y_v (S)	10	-	-
Reshaping coefficient σ	1	-	-

lower (down to 1.1) and higher effective SCR (up to 4.5). The results show that by increasing the SCR the damping increases and vice versa: therefore, the proposed reshaping control designed for weak grid does not degrade the performances of the VSC when the grid becomes stiffer.

In the light of this results, the authors suggest to initialize the grid impedance Z_g, in case of uncertainty, with the *highest value* (resulting in lowest SCR) which it is expected to reach. If the proposed reshaping control is effective at that low SCR value, it will keep its effectiveness also for higher SCR values. Furthermore, the reshaping feedback can be also deactivated in stiff grid condition by simply setting $\sigma = 0$.

The electric grid can also experience supply voltage variation with different entities and duration [38], where the converter injects/absorbs reactive power to regulate its output ac voltage [8]. Under this scenario, the reshaping control operates at a different operating point with respect to the one for which it has been designed ($e = 1$ p.u.). The procedure in Fig. 2 is used to linearize the grid model around different operating points and analyze the dynamics of the reshaping control [7]. The resulting eigenvalue analysis in Fig. 9(a) demonstrates that the damping capability of the reshaping control is not impaired for voltage levels between $e = 0.75$ p.u. and $e = 1.1$ p.u. For $e = 0.75$ p.u. the minimum damping ratio reaches $\zeta = 0.35$, which is still an acceptable value and warranties sufficient stability margins. Voltage levels below $e = 0.7$ p.u. are not present in Fig. 9(a) and not considered in this paper, since for those values the equilibrium point does not exist and the Newton-Raphson algorithm does not converge [17], [32].

The behaviour of the reshaping control for different active power levels P^* is analyzed in Fig. 9(b). It is shown that, when the active power level decreases till $P^* = 0$ p.u., the damping ratio of the VSC with reshaping control reaches $\zeta = 0.35$, which is still an acceptable value. When increasing the power to $P^* = 1.2$ p.u., eigenvalues with natural frequency around 30 Hz decrease their damping to $\zeta = 0.37$. Values higher than $P^* = 1.2$ p.u. are not shown in Fig. 9(b) because they exceed the static maximum power transfer capability [33].

B. Comparison of SISO and MIMO for power system dynamic reshaping

The dynamics of a VSC-based power system is highly dependent on the control systems of the single VSCs [5], [7]. Thus, active damping solutions implemented in the VSCs can potentially introduce beneficial effects also for the power system stability. However, the contribution of different AD solutions on the power system dynamics, in other words, their *dynamic reshaping capability*, has to be quantified.

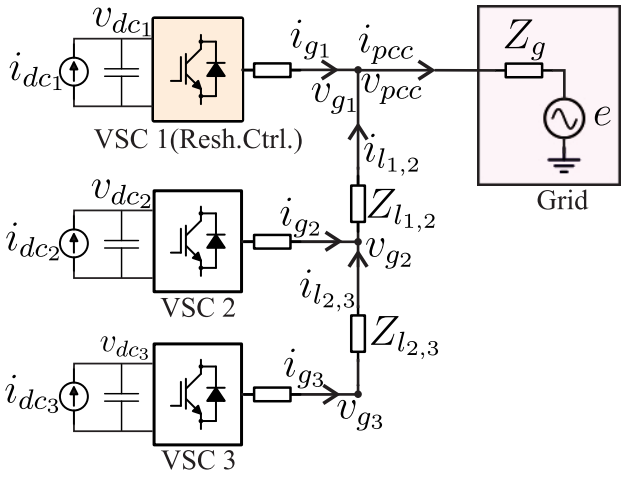

Fig. 10: The model of the considered grid with 3 VSCs. The VSC 1, in orange, implements the reshaping control.

A simple and widely-used SISO active damping strategy was proposed in [9], based on a filtered feedback from the VSC output voltage v_g. The reshaping feedback u in Fig. 1 is thus:

$$u = B(s)Y_v v_g \tag{11}$$

where Y_v is is virtual admittance and $B(s)$ is a bandpass filter for the d and q components of the feedback [9], [14]. This SISO impedance reshaping strategy (11) is compared with the proposed MIMO reshaping control (6) in the VSC-based grid in Fig. 10. A nonlinear state-space model of the considered grid with three different VSCs is derived according to [7]. The main parameters are summarized in Table II. The VSC 1, highlighted in orange, implements the conventional admittance reshaping (11) [9], and the proposed reshaping control (6). The reshaping matrix K is declared in (12). The virtual admittance Y_v and the reshaping coefficient σ are initialized to 0 (no reshaping control), and both progressively increased according to Fig. 11.

The purple eigenvalues in Fig. 11 demonstrates that the admittance reshaping feedback (11) increases the damping of the VSC-based grid, but in a limited amount. The maximum reached damping is $\zeta = 0.2$ for $Y_v = 10$; increasing Y_v over that value makes the eigenvalues move to the right side, making the grid stability worse.

Conversely, the proposed reshaping control can increase the eigenvalues damping (represented in orange) by increasing σ, reaching a damping of $\zeta = 0.32$ for $\sigma = 1$, the 50% more than with conventional impedance reshaping. The higher damping capability of the proposed control has two reasons, clear from the matrix K in (12). Firstly, it uses feedbacks from the dc voltage v_{dc}, and the main control states δ, Φ_{dc}, Φ_g, Φ_q, not used in (11). Secondly, the rows of K in (12) are different,

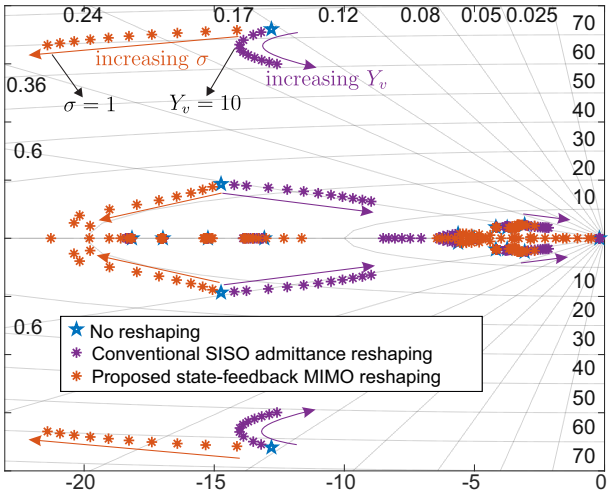

Fig. 11: The effect of conventional (SISO) and proposed (MIMO) reshaping control implemented in the the VSC 1 in Fig. 10 on the eigenvalues of the whole considered power system.

resulting in asymmetric control of u_d and u_q which can better damp the asymmetric dynamics of the main control.

The damping of $\zeta = 0.32$ for $\sigma = 1$ obtained in a VSC-based grid in Fig. 11 is however less than $\zeta = 0.4$ obtained in the single VSC case of Fig. 4. Independently on the used active damping strategy on the VSC 1, its contribution on the grid dynamics is limited, since the VSC 2 and VSC 3 without any implemented AD dictate great part of its dynamics. Thus, conventional AD solutions such as [9] which may introduce sufficient damping in the single VSC case can be insufficient in a multi-VSC weak grids. That motivates the investigation of control solutions with higher damping capability, as the proposed state-feedback reshaping control.

The robustness of the proposed control with respect to a wide range of grid impedance variation, discussed in subsection V-A, allows an effective operation also in presence of other VSCs, which can vary the equivalent grid impedance seen by the converter [39].

VI. Experimental Results

The experimental results are conducted in two parts. At first, the reshaping control is implemented in a down-scaled setup built in the lab, described in Fig. 12 and with parameters declared in Table III. Afterwards, the power system in Fig. 10 is built and simulated in real-time on a Typhoon® 402 Hardware-In-the-Loop (HIL) device with parameters declared in Table II, to test the behavior of the proposed control at power system-level.

TABLE III: Back-to-back converter and power amplifier experimental set-up parameters

Parameters	Fig 13 (weak)	Fig 14 (stiff)
Peak voltage of power amplifier (V)	250	250
Grid inductance Z_g (mH)	35	18
Short Circuit Ratio (SCR)	1.6	3
Nominal active power (kW)	1	1
Switching frequency (kHz)	10	10
Nominal dc-link voltage (V)	600	600
DC-link capacitor (mF)	1.2	1.2
Converter side inductor L_{f_1} (mH)	5	5
Filter capacitor C_f (μF)	15	15
Grid side inductor L_{f_2} (mH)	0.5	0.5

A. Single VSC laboratory tests

In Fig. 12, the inverter of the back-to-back (in orange) is the considered VSC implementing the reshaping control, while the rectifier in the left injects the current i_{dc} into the dc-link, providing the active power $P_{dc} = i_{dc}v_{dc}$ to the inverter. The grid is emulated through a power amplifier connected to the VSC through a series of inductors, as shown in Fig. 12.

In the experiment of Fig. 13, a weak grid with the parameters declared in Table III is built. A quick dc active power P_{dc} drop from 1 kW to 0 kW is applied to the inverter by switching the rectifier off. The conventional control without active damping in Fig. 13(a) presents undamped oscillation in the ac current, dc and ac voltage, dangerous for the stability. Conversely, the proposed reshaping control in Fig. 13(b) can overcome the dc power drop with a significantly higher damping and no oscillations.

The experiment in Fig. 14 is realized with a stiffer grid, as declared in Table III, to demonstrate the robustness of the reshaping control under grid impedance variation, as discussed in subsection V-A. The tuning of the reshaping control is kept the *same* of the previous experiment, and the same P_{dc} disturbance is applied. In the case of conventional control in Fig. 14(a), oscillations in the ac current and dc voltage arises due to the disturbance. The proposed reshaping control in Fig. 14(b) still keeps its damping capability even in stiff grid, and obtains higher performance than the conventional control.

B. System-level reshaping control tests

The power system considered in Fig. 10 is built on a Typhoon® 402 Hardware-In-the-Loop (HIL) device by means of three back-to-back VSC-based wind turbine systems connected in parallel. A time step of 1 μs is used for the real-time simulation, which, for converters with switching frequency of 2 kHz and a state-feedback controller operating at low frequencies, ensures accurate and realistic results. Both the conventional SISO admittance reshaping and the proposed MIMO reshaping control with K declared in (12) are implemented. A dc brake chopper is added in the dc-link to protect it from overvoltage.

In the first experiment in Fig. 15, the VSC 1 and VSC 2 are operating at their nominal power and VSC 3 is initially disabled. The parameters of the experiment are reported in Table II. At the triggering instant ($t = 0$ s), the VSC 3 is enabled and connected in parallel with VSC 1 and 2, initially with null active power from its rectifier ($i_{dc_3} = 0$) to avoid excessive start-up current. In Fig. 15(a), the experiment is realized without any damping strategy. The start-up of the VSC 3 creates a transient disturbance in the grid, which gives birth to growing oscillations which result after 0.5 s in instability and tripping of all the three converters due to dc overvoltage. The breaking chopper installed in the dc-link is activated

$$K = \begin{array}{c} \\ u_d \\ u_q \end{array} \begin{array}{c} \begin{array}{cccccccccc} i_{c_d} & i_{c_q} & v_{dc} & \Phi_{dc} & \Phi_g & \delta & \Phi_q & v_{cc_d} & v_{cc_q} & i_{g_d} & i_{g_q} \end{array} \\ \begin{pmatrix} -0.52 & -0.46 & -23.5 & 205.9 & 3214 & 15819 & 369.89 & -0.16 & 2.64 & 3.24 & 1.36 \\ 2.12 & 1.20 & -22.8 & 4712 & 14480 & 86267 & -262.15 & 3.97 & 23.57 & 1.53 & 7.81 \end{pmatrix} \end{array} \tag{12}$$

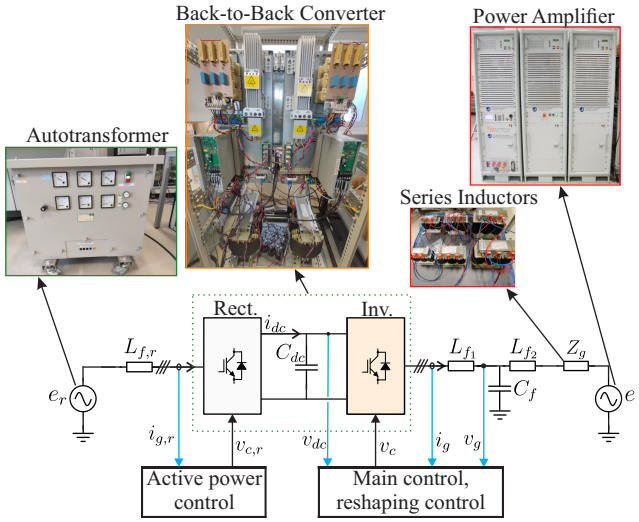

Fig. 12: The back-to-back converter implementing the reshaping control used for the experimental results.

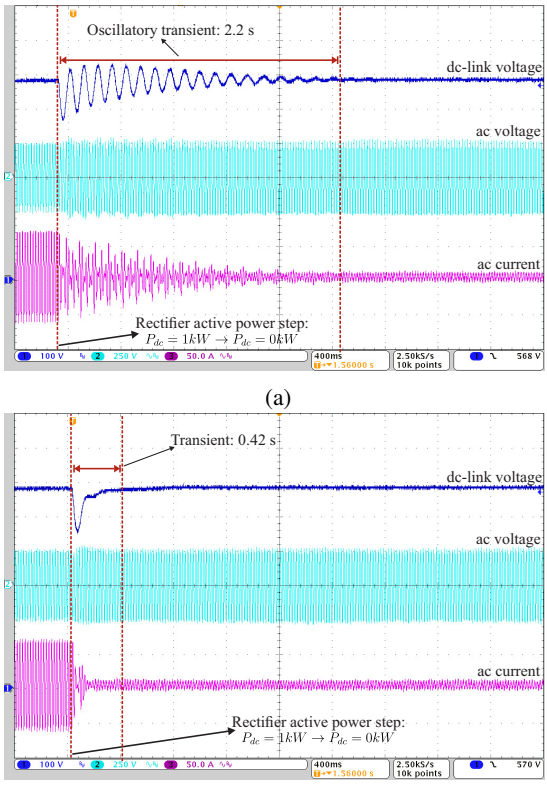

(a)

(b)

Fig. 13: The performances improvements of the proposed reshaping control in weak grid. (a) Conventional multi-loop control. (b) Proposed reshaping control.

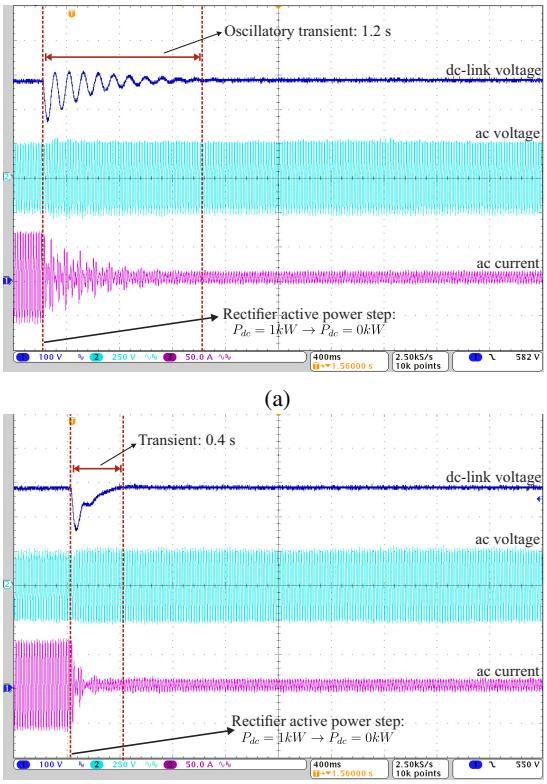

(a)

(b)

Fig. 14: The performances improvements of the proposed reshaping control in stiff grid. (a) Conventional multi-loop control. (b) Proposed reshaping control.

when the dc overvoltage is detected, dissipating the excessive dc power and discharging the dc capacitor, nevertheless it is not sufficient to prevent the converter tripping. The same test has been conducted both with conventional SISO admittance reshaping (11) in Fig. 15(b) and state-feedback reshaping control (6) in Fig. 15(c) operative in VSC 1, and shows in both cases stable operation of the microgrid, with slightly higher damping in the case of state-feedback control.

The performance difference between SISO admittance reshaping (11) and state-feedback reshaping control (6) implemented in the VSC 1 of Fig. 10 is demonstrated in the tests of Figs. 16,17, with all the three VSCs operating at their nominal power. In Fig. 16, a symmetrical voltage sag of 0.25 p.u. with duration 0.5s is applied to the grid supply voltage e, considering the parameters in Table II. The SISO admittance reshaping can damp the oscillation during the voltage dip as shown in Fig. 16(a), nevertheless sustained undamped oscillations in the current, ac and dc voltage arise during the voltage rise. A similar sustained oscillatory phenomena in the near- and sub-synchronous frequency range has been

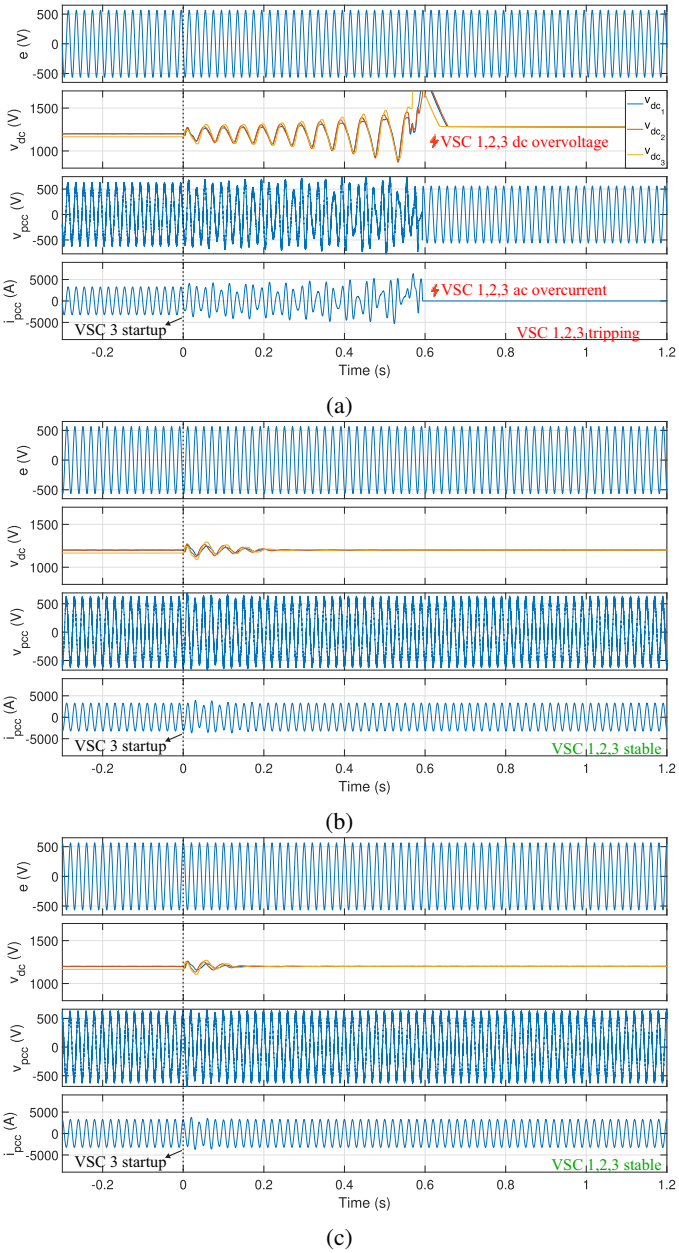

Fig. 15: Startup of the VSC 3 during the operation of VSC 1 and VSC 2. (a) Without reshaping control. (b) With conventional SISO admittance reshaping in VSC 1. (c) With proposed state-feedback MIMO reshaping control in VSC 1.

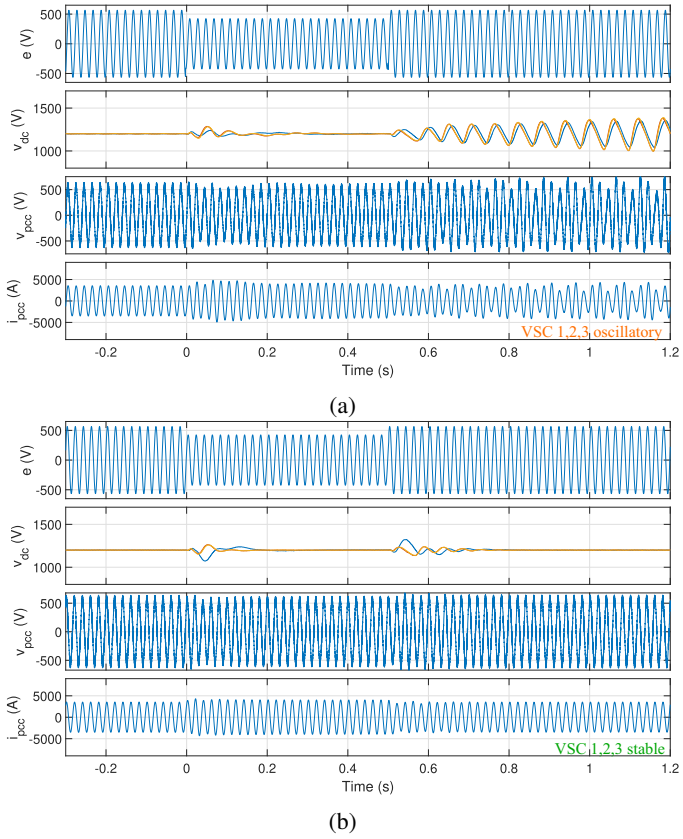

Fig. 16: Test of a voltage sag of 0.25 p.u. with all the three VSCs under operation. (a) With conventional SISO admittance reshaping in VSC 1. (b) With proposed state-feedback MIMO reshaping control in VSC 1.

reported by [1] under the name of harmonic instability, and has been attributed to asymmetrical dynamics of the PLL and the outer control loops in the dq frame. Indeed, traditional SISO impedance reshaping have limited capability to compensate the asymmetric dynamics of the converter control, since in the most of the cases $Y_v(s)$ is chosen equal for the d and q channels [9], [14], [21]. Conversely, the proposed feedback is asymmetric and multi-variable, as clear from (12), and can better damp the dynamics of the asymmetric dq control and cross-coupled outer loops, resulting in more stable microgrid operation, as shown in Fig. 16(b) [1], [7].

In Fig. 17, a rapid frequency increase of 2 Hz with duration 0.5s is applied to the grid supply voltage e, always considering the parameters in Table II. Such rapid frequency variations are possible in low inertia grids dominated by power converters, and caused in the last years well-documented incidents [40], [41]. In Fig. 17(a) with conventional SISO impedance reshaping, undamped oscillations in the current, ac and dc voltage arise during the frequency rise and persist also when the frequency decreases back to the nominal value. The proposed state-feedback reshaping control of Fig. 17(b) can instead damp the oscillations and ensure a stable and effective power system operation, demonstrating superior damping capability than the conventional SISO impedance reshaping.

VII. Conclusions

In this paper, a state-feedback reshaping control is proposed to realize active damping of low frequency power system oscillations, arising from the connection of grid-following converters to ultra-weak ac grids (SCR down to 1.3). Analytic and experimental results demonstrate a 50% higher damping capability of the proposed solution with respect to virtual admittance-based solutions. The design of the proposed control is realized through a systematic offline algorithm which makes it simple, flexible and user-friendly. The proposed control has been tested in parallel operation with other two converters, under external disturbances both from the ac and dc converter

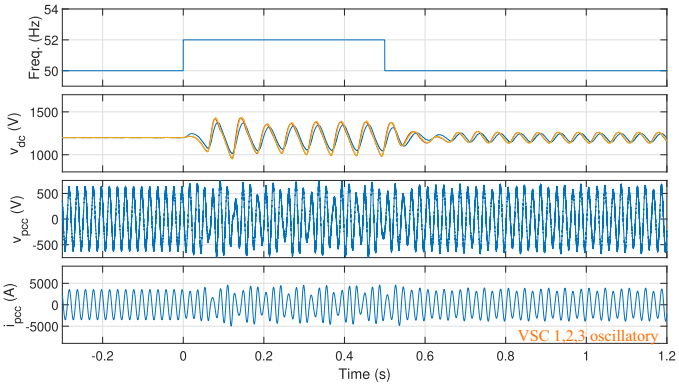

(a)

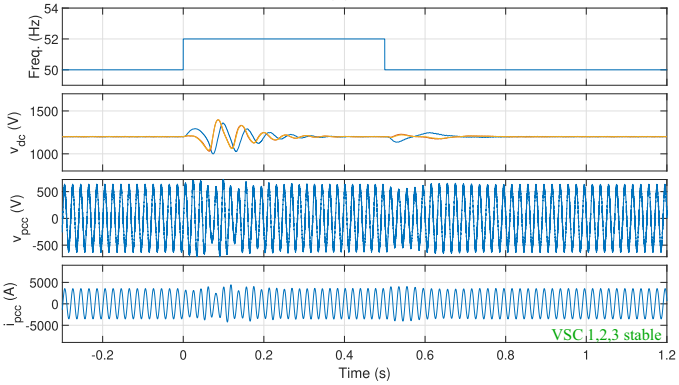

(b)

Fig. 17: Test of a frequency increase of 2 Hz with all the three VSCs under operation. (a) With conventional SISO admittance reshaping in VSC 1. (b) With proposed state-feedback MIMO reshaping control in VSC 1.

side and under SCR variations going from ultra-weak (SCR = 1.3) to stiff grid (SCR = 3) conditions, demonstrating high damping performances in situations where conventional solutions are not effective.

REFERENCES

[1] X. Wang and F. Blaabjerg, "Harmonic stability in power electronic-based power systems: Concept, modeling, and analysis," *IEEE Trans. Smart Grid*, vol. 10, no. 3, pp. 2858–2870, May. 2019.

[2] R. Teodorescu, M. Liserre, and P. Rodriguez, *Grid converters for photovoltaic and wind power systems*, vol. 29. John Wiley & Sons, 2011.

[3] C. Zhang, X. Wang, and F. Blaabjerg, "Analysis of phase-locked loop influence on the stability of single-phase grid-connected inverter," in *2015 IEEE 6th International Symposium on Power Electronics for Distributed Generation Systems (PEDG)*, pp. 1–8. IEEE, 2015.

[4] H. Yuan, X. Yuan, and J. Hu, "Modeling of grid-connected vscs for power system small-signal stability analysis in dc-link voltage control timescale," *IEEE Trans. Power Syst.*, vol. 32, no. 5, pp. 3981–3991, 2017.

[5] N. Pogaku, M. Prodanovic, and T. C. Green, "Modeling, analysis and testing of autonomous operation of an inverter-based microgrid," *IEEE Trans. Power Electron.*, vol. 22, no. 2, pp. 613–625, 2007.

[6] Y. Huang and D. Wang, "Effect of control-loops interactions on power stability limits of vsc integrated to ac system," *IEEE Transactions on Power Delivery*, vol. 33, DOI 10.1109/TPWRD.2017.2740440, no. 1, pp. 301–310, 2018.

[7] F. Cecati, R. Zhu, M. Liserre, and X. Wang, "Nonlinear modular state-space modeling of power-electronics-based power systems," *IEEE Transactions on Power Electronics*, DOI 10.1109/TPEL.2021.3127746, pp. 1–1, 2021.

[8] L. Harnefors, M. Bongiorno, and S. Lundberg, "Input-admittance calculation and shaping for controlled voltage-source converters," *IEEE Trans. Ind. Electron.*, vol. 54, no. 6, pp. 3323–3334, Dec. 2007.

[9] K. M. Alawasa, Y. A. I. Mohamed, and W. Xu, "Active mitigation of subsynchronous interactions between pwm voltage-source converters and power networks," *IEEE Trans. Power Electron.*, vol. 29, no. 1, pp. 121–134, 2014.

[10] X. Zhang, D. Xia, Z. Fu, G. Wang, and D. Xu, "An improved feed-forward control method considering pll dynamics to improve weak grid stability of grid-connected inverters," *IEEE Transactions on Industry Applications*, vol. 54, DOI 10.1109/TIA.2018.2811718, no. 5, pp. 5143–5151, 2018.

[11] D. Yang, X. Wang, F. Liu, K. Xin, Y. Liu, and F. Blaabjerg, "Symmetrical pll for siso impedance modeling and enhanced stability in weak grids," *IEEE Transactions on Power Electronics*, vol. 35, DOI 10.1109/TPEL.2019.2917945, no. 2, pp. 1473–1483, 2020.

[12] F. Cecati, R. Zhu, M. Liserre, and X. Wang, "State-feedback-based low-frequency active damping for vsc operating in weak-grid conditions," in *2020 IEEE Energy Conversion Congress and Exposition (ECCE)*, DOI 10.1109/ECCE44975.2020.9235338, pp. 4762–4767, 2020.

[13] Y. Gui, X. Wang, F. Blaabjerg, and D. Pan, "Control of grid-connected voltage-source converters: The relationship between direct-power control and vector-current control," *IEEE Industrial Electronics Magazine*, vol. 13, no. 2, pp. 31–40, 2019.

[14] K. M. Alawasa and Y. A.-R. I. Mohamed, "A simple approach to damp ssr in series-compensated systems via reshaping the output admittance of a nearby vsc-based system," *IEEE Transactions on Industrial Electronics*, vol. 62, no. 5, pp. 2673–2682, 2014.

[15] R. C. Dorf and R. H. Bishop, *Modern control systems*. Pearson, 2011.

[16] G. F. Franklin, J. D. Powell, A. Emami-Naeini, and J. D. Powell, *Feedback control of dynamic systems*, vol. 3. Addison-Wesley Reading, MA, 1994.

[17] H. Wu and X. Wang, "Design-oriented transient stability analysis of pll-synchronized voltage-source converters," *IEEE Trans. Power Electron.*, vol. 35, no. 4, pp. 3573–3589, 2019.

[18] H. Gong, X. Wang, and L. Harnefors, "Rethinking current controller design for pll-synchronized vscs in weak grids," *IEEE Transactions on Power Electronics*, vol. 37, no. 2, pp. 1369–1381, 2021.

[19] F. Zhao, X. Wang, and T. Zhu, "Power dynamic decoupling control of grid-forming converter in stiff grid," *IEEE Transactions on Power Electronics*, DOI 10.1109/TPEL.2022.3156991, pp. 1–1, 2022.

[20] F. Cecati, M. Liserre, Y. Liao, X. Wang, and F. Blaabjerg, "Design oriented analysis of control loops interaction in power synchronization-based voltage source converter," in *2021 IEEE Energy Conversion Congress and Exposition (ECCE)*, DOI 10.1109/ECCE47101.2021.9595531, pp. 3282–3288, 2021.

[21] X. Wang, Y. W. Li, F. Blaabjerg, and P. C. Loh, "Virtual-impedance-based control for voltage-source and current-source converters," *IEEE Trans. Power Electron.*, vol. 30, DOI 10.1109/TPEL.2014.2382565, no. 12, pp. 7019–7037, 2015.

[22] J. Fang, X. Li, H. Li, and Y. Tang, "Stability improvement for three-phase grid-connected converters through impedance reshaping in quadrature-axis," *IEEE Transactions on Power Electronics*, vol. 33, no. 10, pp. 8365–8375, 2017.

[23] B. Hu, H. Nian, M. Li, and Y. Xu, "Impedance characteristic analysis and reshaping method of dfig system based on dpc without pll," *IEEE Transactions on Industrial Electronics*, vol. 68, no. 10, pp. 9767–9777, 2020.

[24] F. Deng, Y. Li, X. Li, W. Yao, X. Zhang, and P. Mattavelli, "A decentralized impedance reshaping strategy for balanced, unbalanced and harmonic power sharing in islanded resistive microgrids," *IEEE Transactions on Sustainable Energy*, vol. 13, no. 2, pp. 743–754, 2021.

[25] L. Huang, H. Xin, and F. Doerfler, "H infinity control of grid-connected converters: Design, objectives and decentralized stability certificates," *IEEE Trans. on Smart Grid*, vol. 11, no. 5, pp. 3805–3816, 2020.

[26] M. Chen, D. Zhou, A. Tayyebi, E. Prieto-Araujo, F. Doerfler, and F. Blaabjerg, "Generalized multivariable grid-forming control design for power converters," *IEEE Transactions on Smart Grid*, DOI 10.1109/TSG.2022.3161608, pp. 1–1, 2022.

[27] Y. Huang, X. Yuan, J. Hu, and P. Zhou, "Modeling of vsc connected to weak grid for stability analysis of dc-link voltage control," *IEEE Journal of Emerging and Selected Topics in Power Electronics*, vol. 3, DOI 10.1109/JESTPE.2015.2423494, no. 4, pp. 1193–1204, 2015.

[28] J. Kautsky, N. K. Nichols, and P. Van Dooren, "Robust pole assignment in linear state feedback," *Int. J. Control*, vol. 41, no. 5, pp. 1129–1155, 1985.

[29] D. Dong, B. Wen, D. Boroyevich, P. Mattavelli, and Y. Xue, "Analysis of phase-locked loop low-frequency stability in three-phase grid-connected power converters considering impedance interactions," *IEEE Trans. Ind. Electron.*, vol. 62, no. 1, pp. 310–321, Jan. 2015.

[30] L. J. et al., "Measurement results and performance analysis of the grid impedance in different low voltage grids for a wide frequency band to support grid integration of renewables," in *2015 IEEE Energy Conversion Congress and Exposition (ECCE)*, pp. 1960–1967, 2015.

[31] F. Cecati, R. Zhu, M. Langwasser, M. Liserre, and X. Wang, "Scalable state-space model of voltage source converter for low-frequency stability analysis," in *2020 IEEE Energy Conversion Congress and Exposition (ECCE)*, pp. 6144–6149, 2020.

[32] A. M. Kettner, L. Reyes-Chamorro, J. K. Maria Becker, Z. Zou, M. Liserre, and M. Paolone, "Harmonic power-flow study of polyphase grids with converter-interfaced distributed energy resources - part i: Modeling framework and algorithm," *IEEE Transactions on Smart Grid*, vol. 13, DOI 10.1109/TSG.2021.3120108, no. 1, pp. 458–469, 2022.

[33] X. Wang, M. G. Taul, H. Wu, Y. Liao, F. Blaabjerg, and L. Harnefors, "Grid-synchronization stability of converter-based resources - an overview," *IEEE Open Journal of Industry Applications*, vol. 1, DOI 10.1109/OJIA.2020.3020392, pp. 115–134, 2020.

[34] Q. Hu, L. Fu, F. Ma, and F. Ji, "Large signal synchronizing instability of pll-based vsc connected to weak ac grid," *IEEE Transactions on Power Systems*, vol. 34, DOI 10.1109/TPWRS.2019.2892224, no. 4, pp. 3220–3229, 2019.

[35] S. M. Toolbox *et al.*, "Matlab," *Mathworks Inc*, 1993.

[36] X. Wang, L. Harnefors, and F. Blaabjerg, "Unified impedance model of grid-connected voltage-source converters," *IEEE Trans. Power Electron.*, vol. 33, no. 2, pp. 1775–1787, 2018.

[37] H. Wang, C. Buchhagen, and J. Sun, "Methods to aggregate turbine and network impedance for wind farm resonance analysis," *IET Renewable Power Generation*, vol. 14, no. 8, pp. 1304–1311, 2020.

[38] "Ieee recommended practice for monitoring electric power quality," *IEEE Std 1159-2019 (Revision of IEEE Std 1159-2009)*, DOI 10.1109/IEEESTD.2019.8796486, pp. 1–98, 2019.

[39] X. Wang, F. Blaabjerg, and W. Wu, "Modeling and analysis of harmonic stability in an ac power-electronics-based power system," *IEEE Trans. Power Electron.*, vol. 29, no. 12, pp. 6421–6432, 2014.

[40] A. Derviškadić, G. Frigo, and M. Paolone, "Beyond phasors: Continuous-spectrum modeling of power systems using the hilbert transform," *arXiv preprint arXiv:1906.11154*, 2019.

[41] R. Yan, N.-A. Masood, T. Kumar Saha, F. Bai, and H. Gu, "The anatomy of the 2016 south australia blackout: A catastrophic event in a high renewable network," *IEEE Transactions on Power Systems*, vol. 33, DOI 10.1109/TPWRS.2018.2820150, no. 5, pp. 5374–5388, 2018.